Mech Time-Depend Mater (2011) 15: 105–117
DOI 10.1007/s11043-010-9127-4

Tissue and microstructural deformations in aortic tissue under stretch and after deformation recovery

Danial Shahmirzadi · Adam H. Hsieh

Received: 7 July 2010 / Accepted: 1 December 2010 / Published online: 17 December 2010

Abstract Elucidating how cardiovascular biomechanics is regulated during health and disease is critical for developing diagnostic and therapeutic methods. The extracellular matrix of cardiovascular tissue is composed of multiple fibrillar networks embedded in an amorphous ground substance and has been found to reveal time-dependent mechanical behavior. Given the multiscale nature of tissue biomechanics, an accurate description of cardiovascular biomechanics can be obtained only when microstructural morphology is characterized and put together in correlation with tissue-scale mechanics. In this study, we sought to determine how the microstructural configuration in aortic tissue changes with tissue-scale loading protocols. At the tissue level, rather intuitively, the width and thickness decrease when specimens undergo elongation and it is found that there is a higher inverse correlation between the elongation of circumferential specimens and the shrinkage along the thickness than along the width. After deformation recovery, the specimens show levels of permanent deformation in both thickness and width as neither recovers the initial values for the unstretched specimen, with higher permanent deformation measured for thickness. At the microstructural level, the networks in the wall inner layer show straighter fibrillar structure under stretch, which partly returns to the crimping structure after deformation recovery. This study indicates a microstructural basis for observations of regional permanent tissue stretch in artery tissues, and furnishes early data for developing multiscale models of cardiovascular viscoelastic/viscoplastic modeling.

Keywords Microstructural deformation · Multiscale modeling · Matrix-solid interaction · Cardiovascular biomechanics

D. Shahmirzadi (✉)
Department of Mechanical Engineering, University of Maryland, College Park, MD 20814, USA
e-mail: dshahmir@umd.edu

D. Shahmirzadi · A.H. Hsieh
Fischell Department of Bioengineering, University of Maryland, College Park, MD 20814, USA

A.H. Hsieh
e-mail: hsieh@umd.edu

1 Introduction

A large portion of the biological soft tissues exhibit multiscale biomechanics in which the mechanical behavior of the tissue has characteristics deriving from microstructural components (Lillie 1986; He and Roach 1994; Weinberg et al. 2010). Characteristic changes in tissue fibrillar structure can potentially serve as an early diagnostic marker in various pathological processes which, in turn, necessitates establishing more precise measures of quantifying the tissue microstructure (Weibel 1989; Roberts et al. 2000; Erikson et al. 2007). Unlike at tissue-scale, where measuring a specimen's dimensions can provide a sufficient description of tissue deformation, quantification of microstructural deformations is a challenge (Avolio et al. 1998) and has been one of the principal areas of advancement in experimental biology over the past decade (Bolender 1992).

Most of the traditional methods for assessing tissue microstructure have been limited to providing qualitative or semi-numerical assessments of the microstructure (Knodell et al. 1981; Ishak et al. 1995; Brunt 2000; Dahab et al. 2004) assessed at random states of tissue deformation aimed at detecting tissue composition. It is difficult to develop highly reproducible and standardized qualitative measures for assessing microstructural configuration (Kage et al. 1997). A traditional and commonly practiced approach to studying the microstructural morphology in soft issues is through analyzing the histology images obtained under the microscope (Castleman 1996; Amenabar et al. 2006).

The majority of the studies relevant to the identification of changes in tissue histology during different healthy and diseased conditions, however, have focused on characterizing the quantity and density of certain tissue components but not so much on their orientation. The collagen fibrillar content in liver tissue, regardless of its orientation, has been quantified for studying chronic liver diseases (Sun et al. 2008). Besides the content and density of tissue structural components, a key factor in determining tissue biomechanics is the orientation of fibrillar networks. Few studies exist whose goal was to characterize the fibrillar orientation in tissue microstructure. Rubbens et al. quantified collagen orientation in engineered cardiovascular tissue images using an innovative eigen-value based analysis (Tonar et al. 2003; Daniels et al. 2006; Rubbens et al. 2009).

In this study, we sought to examine the tissue histology under systematic and predefined loading protocols and study the directionality of microstructural configurations at each loading state. The results of this study were used to establish the platform for further quantifications of the tissue microstructure using image-based techniques (Shahmirzadi and Hsieh 2009a, submitted (a)).

2 Materials and methods

2.1 Specimen preparation

Aortas of 291 ± 23 mm length were obtained from Angus male cattle (average age of 20–24 months) at a local abattoir. Each aorta was cut proximally near the heart and distally above the abdominal bifurcation, and was immersed in cold phosphate buffered saline (PBS) while transferred to the laboratory. The tissue was carefully cleaned of large remnants of fat and attached connective tissues. Only one third of the tissue at the proximal end was used in order to minimize potential region-dependent discrepancies in tissue properties. Areas of the aorta containing vascular branch points and abnormalities were discarded.

Given the dominant circumferential orientation of structural networks in the aorta, rectangular specimens were cut and tested along the circumferential direction. If the aorta

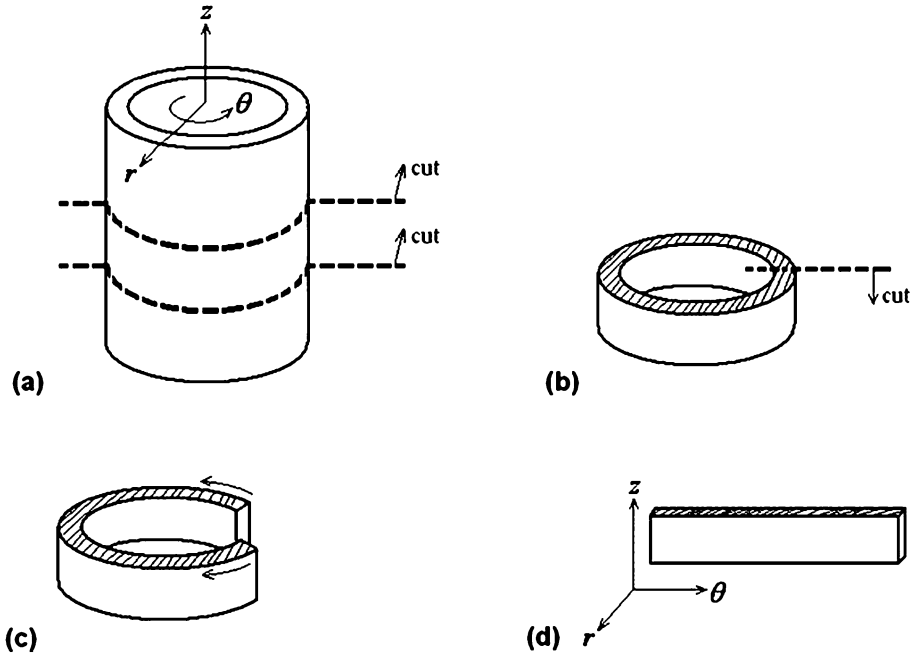

Fig. 1 Representation of coordinate systems on the aorta and cut specimens as well as the schematic steps involved in cutting the specimens

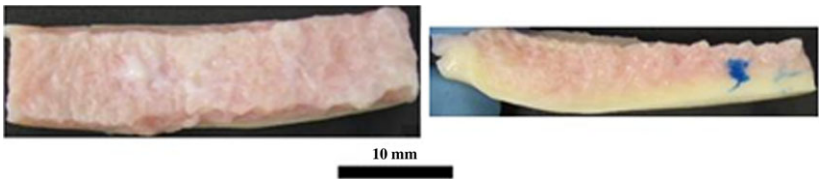

Fig. 2 (Color online) Pictures of cut circumferential specimen: right-top view, left-side view. On the side view, the *blue dot* shows the mark of tissue dye used to measure thickness on the image

was schematically considered to be a cylinder with the cylindrical polar coordinate system, $r-\theta-z$, set as shown in Fig. 1(a), the coordinate system on the circumferential specimens is shown in Fig. 1(d). Schematic of the main steps in cutting the specimens out of the aorta are also represented in the figure. The template was set to give specimens with 30 mm $\times$10 mm length by width dimensions, and the thicknesses naturally varying in the 3–8 mm range, Fig. 2. Extra care was paid to excise specimens in the circumferential direction in order to be able to identify the circumferential direction throughout the later stages under the microscope and the histological examinations. The excised specimens were preserved in PBS solution with protease-inhibitor additives (per 1 Liter of PBS: 1 mM of EDTA-Disodium salt, 1 mM of EDTA-Tetrasodium salt, 5 mM of Benzamadine, 10 mM of NEM, 1 mM of PMSF) until being used. The compounds were added in order to inhibit enzymatic degradation of proteins by making it unfavorable for matrix-degrading enzymes to function. The additives should affect neither the mechanical properties nor the proteins of the tissue in any way (Samouillan et al. 2000).

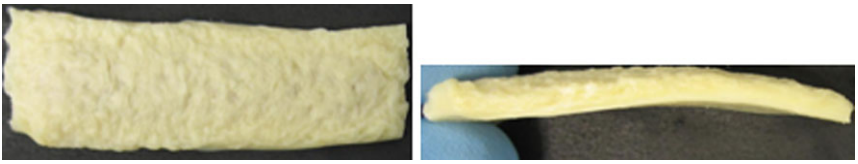

Fig. 3 Pictures of elastin-isolated specimen: right-top view, left-side view

2.2 Isolation of elastin

Since elastin is believed to play a major role in giving the arterial tissue its viscoelastic properties (Fung 1993; Humphrey 1999), experiments were also performed on tissues treated to remove non-elastin tissue constituents. A group of native tissue specimens was initially treated in order to denature collagen and other proteins in the extracellular matrix, leaving the elastin intact. These specimens were prepared to examine the effects of extracellular matrix integrity on the tissue mechanical behavior. Specimens from native tissue were autoclaved for 1 hour under chamber pressure of $p = 15$ psi ($\approx$103 KPa) (Pezzin et al. 1976; Weinberg et al. 1995; Lillie et al. 1996). The autoclaving pressure of 15 psi was associated with the corresponding superheated temperature of $T = 115°\text{C}$. Superheating the tissue proteins causes them to denature. However, because the denaturation temperature for collagen is about $T_d \approx 40°\text{C}$–$63°\text{C}$ (Fung 1993; Samouillan et al. 2000), compared to $T_d \approx 200°\text{C}$ for elastin (Pezzin et al. 1976), heating the tissue up to around $T = 115°\text{C}$ only causes collagen denaturation but not elastin. Since denaturation is an irreversible process (Wright and Humphrey 2002), by cooling down the tissue, the collagen proteins do not reassemble. It has also been found that the mechanical properties of elastin do not markedly change during the heating and cooling processes (Fung 1993; Lillie et al. 1994). Superheating the tissue also kills the smooth muscle cells (Humphrey 1999). Based on preliminary histological examination, the heat-denatured specimens possess extracellular matrix proteins within an intact elastin network. It is expected that the remnants of denatured proteins lack specific structural interactions with the elastin network, but rather act as bulk material within pores of this network.

The heat-denatured specimens were further processed by extraction in 0.1 M NaOH for 1 hour under temperature of $T = 98°\text{C}$ to remove proteoglycans from the autoclaved specimens (Pezzin et al. 1976) and to further eliminate remnants of denatured collagen (Samouillan et al. 2000; Brzezinski et al. 2007). At this point, the treated tissue is essentially composed of isolated elastin, as confirmed by histology. No positive staining for collagen or proteoglycans is detectable (see Figs. 10 and 11). Figure 3 shows top and side images of an elastin-isolated specimen. Because specimens are free from other protein material, pores in the elastin network are filled with fluid, which is expected to have no contribution on the steady-state mechanics of the tissue.

2.3 Deformation control device

A customized apparatus was designed and manufactured in order to retain tissue specimens under a controlled deformation state over time. The apparatus consists of one stand and two movable jigs which can be screw-secured on the stand. The stand contains a set of holes at measured locations which allow adjustment of the jigs on the stand with a specific distance between them. To load the specimen on the apparatus, the jigs were first secured on the stand at 1.0 inch apart from each other. The specimen was placed in between the two wings

of each jig and the wings were screwed close until they applied enough force to tightly grab the ends of the specimen, but not too tight to squeeze the specimen and damage the tissue integrity. After the specimen was secured between jigs, one jig was unscrewed from the stand and screwed to the new position of interest, i.e. 2.0 inch, if $\lambda = 2$ is needed. For specimens to be examined under stretch, the apparatus and the specimen—under stretch—were left in a 500 ml beaker containing tissue fixative for 24 hours. For specimens to be examined after deformation recovery, the apparatus and the specimen—under stretch—were first placed in PBS for 45 minutes in order for stress relaxation to take place in the tissue. Our separate studies on biomechanics of same specimens indicated that the stress relaxation at tissue-scale completes in less than 20 minutes (Shahmirzadi et al. submitted (b)), so we believe that the same time range should be enough for relaxation to complete in microstructural level. One end of the specimen was then released from the jig so it could retract to the new unloaded state. Letting the stress relaxation takes place in tissue specimens helps obtaining a more reliable representation of average tissue microstructure under stretch. Stress relaxation causes a more uniform and homogenized microstructure with minimum local and abrupt deformations. Specimens were finally left in a modified fixative solution consisting of 10% Clorox® and 15% Formaldehyde in deionized water for 24 hours to fix the microstructure (Shahmirzadi and Hsieh 2009b, 2010). It has been reported that Clorox® and Formaldehyade show better fixation properties for certain tissue components, primarily elastin and collagen, respectively (Hopwood 1967; Lillie et al. 1996). To avoid having confounding effects due to lack of knowledge on the kinetics of chemical fixation, a steady state stress/strain is attained before tissues are fixed.

2.4 Dimension measurement

To examine the macroscale changes in the tissue, the dimensions of the specimens were obtained at each of the loading steps of unstretched, under stretch and after deformation recovery. Given the extraction of the specimens along the circumferential direction of the aorta, comparing the change in specimen width and thickness during sample elongation can be a partial indicator for different mechanisms of, respectively, in-layer versus cross-layer fibrillar deformations in the tissue. The width and thickness of tissue specimens were measured on the calibrated images taken from top and side views of the specimens (Shahmirzadi and Hsieh 2010).

2.5 Histological examinations

Histological examinations are those to study the microstructure of the tissue. Tissue processing machine was used to prepare the tissue by dehydration of the tissue by ethanol, removing the ethanol by Xylene and infiltrating the paraffin into the microstructure of the tissue. Then paraffin-embedding machine was used to produce a clear-cut block of paraffin enclosing the paraffin-infiltrated specimen. Blocks of paraffin encompassing the tissue specimens were sectioned to extract sections of 6 μm–10 μm thickness. The fibrillar microstructure of aortic tissue is organized into lamellas laid tilted around the circumferential orientation, shown as θ in the cylindrical coordinate system. Our own observations showed that among the three possible planes in this coordinate system, the r–θ plane was the best plane for preparing histological sections since it provides the most intact and clear observation on the fibrillar structure and orientation (not shown here). Slides of tissue microstructure were stained using a protocol which was a customized modification of Masson's trichrome with Verhoeff's hematoxylin (Sheehan and Hrapchak 1980; Gravey et al. 1991), who stains elastin in dark blue, collagen in light blue, and proteoglycans in red, Fig. 4. Stained sections of tissue histology were studied under the microscope to detect microstructural configurations.

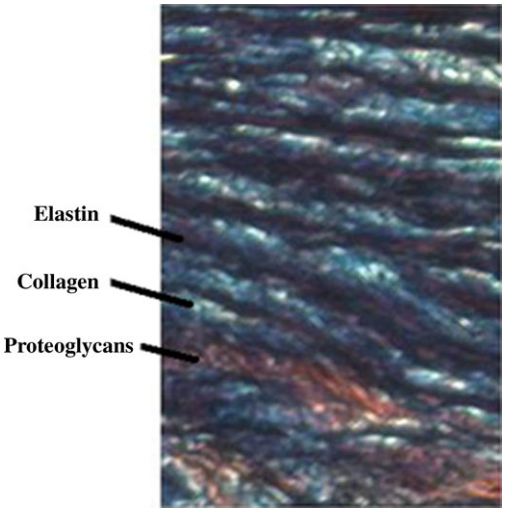

Fig. 4 (Color online) Histological examinations stained with modified Masson's trichrome protocol with Verhoeff's hematoxylin (elastin in *dark blue*, collagen in *light blue* and proteoglycans in *red*)

Table 1 Measurements on width and thickness of tissue specimens at different states of loading

		Unstretched	Stretched $\lambda = 1.4$	Stretched $\lambda = 2.0$	Recovered $\lambda = 1.4$	Recovered $\lambda = 2.0$
Native	Width	15.31	14.21	12.70	14.75	12.82
	Thickness	6.30	4.62	4.06	5.80	4.91
Elastin-Isolated	Width	14.83	12.97	–	13.60	–
	Thickness	3.58	2.98	–	3.32	–

3 Results

3.1 Tissue—scale changes

Table 1 shows the average of the measurements on width and thickness of specimens from both native and elastin—isolated tissue when extended to stretches of 1.4 and 2.0 as well as after being recovered from each of the stretch levels. The specific stretch magnitudes were chosen to describe tissue deformation under both physiological and supra-physiological conditions for aortic tissue (Apter 1967; Hoeve and Flory 1958; Lillie et al. 1996). Width and thickness data are represented in Fig. 5. Bars for data sets that are statistically different are connected with brackets. Table 2 shows the width and thickness measurements on both native and elastin-isolated tissues under stretch and after deformation recovery, normalized to measurements on the unstretched specimens.

One interesting observation is the inward bending of the specimens when released for deformation recovery, Fig. 6, likely due to higher recovery of deformation toward the inner layers of wall thickness, which have larger elastin density, when compared to outer layers.

3.2 Histological observations at different sectioning planes

An interesting observation made through histological slides was the change in the orientation of the fibrillar structure across the wall layer. Figure 7 shows histology images of specimens

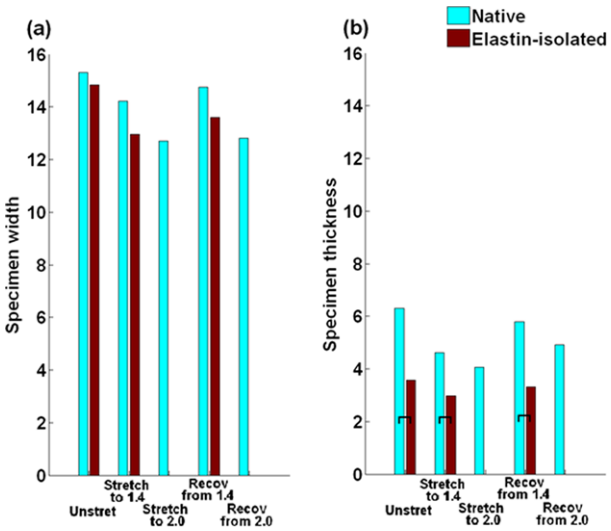

Fig. 5 Change in (**a**) width, (**b**) thickness of specimens under different loading states sorted for native and elastin-isolated tissues. *Bars* for data sets that are statistically different are connected with *brackets*

Table 2 Relative change in width and thickness of tissue specimens during loading and unloading normalized for measurements on unstretched specimens

		Stretched $\lambda = 1.4$	Stretched $\lambda = 2.0$	Recovered $\lambda = 1.4$	Recovered $\lambda = 2.0$
Native	Width	0.91	0.85	0.95	0.86
	Thickness	0.72	0.66	0.90	0.80
Elastin-Isolated	Width	0.87	–	0.92	–
	Thickness	0.83	–	0.93	–

under no stretch, under stretch and after deformation recovery, sectioned in both the r–θ and r–z planes (see Fig. 1(d) for coordinates on the circumferential specimen). It is observed that the dominant orientation of the fibrillar network toward the very inner layer (intima) is along the z direction and by moving toward the media layer it abruptly changes to be along the θ direction. This observation is particularly evident when comparing corresponding histology images at two different planes in Fig. 7.

3.3 Histology of native tissue

Particular consideration was paid to the change in microstructural configurations during tissue deformation by looking at histology images from unstretched specimens, specimens under stretch and specimens after deformation recovery. Given the expected difference between inner layers and outer layers of the wall thickness due to the higher density of elastin toward the inner layers, histological images are considered separately for each region. Figures 8 and 9 show the histology sections from respectively inner and outer regions of specimen from native tissue. In each figure, (a) shows the microstructure of the unstretched specimen, (b) shows the microstructure of the specimen stretched to 1.4, (c) shows the microstructure of the specimen after recovery from 1.4 stretch, (d) shows the microstructure

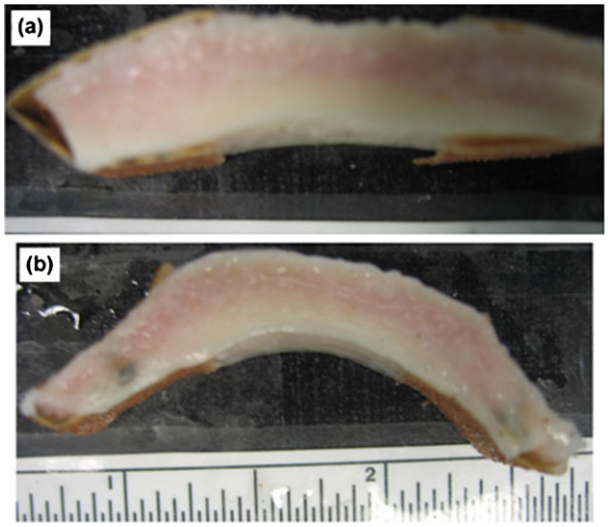

Fig. 6 Side images of a tissue specimen (**a**) before loading, (**b**) after deformation recovery. Inward bending of the specimens after deformation recovery is likely due to the higher deformation recovery toward the inner layer caused by higher elastin density

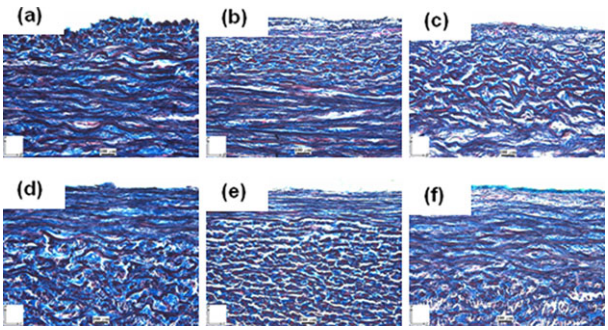

Fig. 7 Histology images of aortic tissue (**a**) r–θ section of unstretched specimen, (**b**) r–θ section of specimen under stretch, (**c**) r–θ section of specimen after deformation recovery, (**d**) r–z section of unstretched specimen, (**e**) r–z section of specimen under stretch, (**f**) r–z section of specimen after deformation recovery

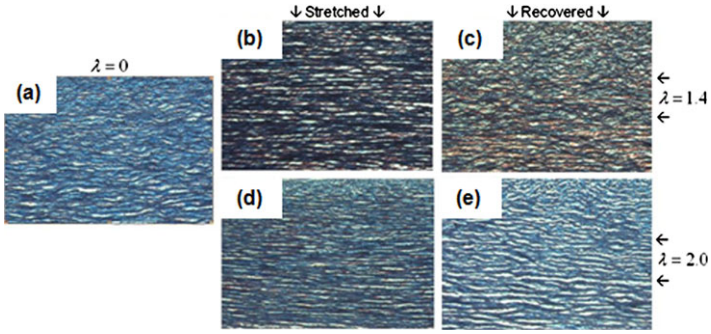

Fig. 8 Histology of specimens from wall "inner" thickness of "native" tissue. (**a**) Unloaded; (**b**) under 1.4 stretch; (**c**) under 2.0 stretch; (**d**) after recovery from 1.4 stretch; (**e**) after recovery from 2.0 stretch

of the specimen stretched to 2.0 and (e) shows the microstructure of the specimen after recovery from 2.0 stretch.

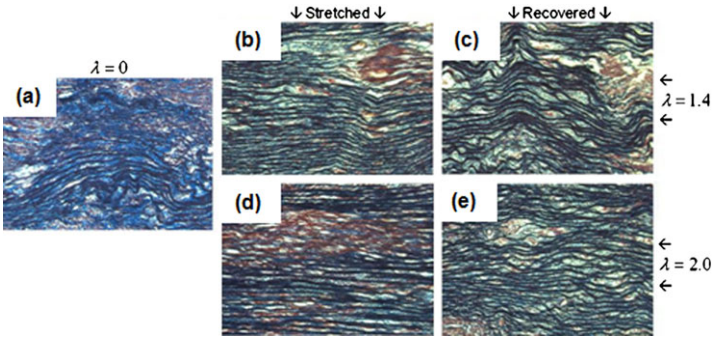

Fig. 9 Histology of specimens from wall "outer" thickness of "native" tissue. (**a**) Unloaded; (**b**) under 1.4 stretch; (**c**) under 2.0 stretch; (**d**) after recovery from 1.4 stretch; (**e**) after recovery from 2.0 stretch

3.4 Histology of elastin-isolated tissue

The specimens from elastin-isolated tissue were only examined under low stretch because loosing the collagen drastically decreases their strength and they were not able to tolerate higher stretch. Figures 10 and 11 show the histology sections from respectively inner and outer regions of specimen from elastin-isolated tissue. In each figure, (a) shows the microstructure of the unstretched specimen, (b) shows the microstructure of the specimen stretched to 1.4 and (c) shows the microstructure of the specimen after recovery from 1.4 stretch.

4 Concluding remarks and discussions

The main goal of this study was to explore the microstructural changes in the tissue when it undergoes deformation; along with relevant changes in tissue-scale dimensions. The histological and tissue-scale measurements were made on the circumferential specimens from the native and elastin-isolated tissue specimens. In studying the tissue microstructural configurations, it should be noted that the potential effects from residual stress in the tissue are not considered. It is known that when unloaded, the aorta maintains the residual stress inside the wall thickness and it is released when the aorta is cut axially (Bergel 1960; Vaishnav and Vossoughi 1987; Vosoughi et al. 1993). In the protocol adapted here to prepare the circumferential specimens, the residual stress inside the ring piece is relieved when the ring is cut axially, and that causes the cut ring to open up into an arch (Shahmirzadi et al. 2008). The argument here is that the microstructural conformations in the tissue might change first during the release of residual stress. Therefore, what we consider as an unstretched specimen might not really represent the microstructure of unstretched aortic tissue, but that of a residual stress-free tissue. Having in mind the distinction between stress-free and load-free aorta caused by the residual stress, the analysis in this chapter is valid for the stress-free aorta, and the stretched and deformation recovered states are evaluated relative to the unstretched state. We did not examine stretch levels smaller than 1.4, since we were interested particularly in the physiologic and supraphysiologic ranges of aorta deformation. There are few rare situations during which an aorta would be loaded below physiologic levels.

Based on the macro-scale examinations, the rather intuitive observation was that the circumferential specimens shrink along both thickness and width when they undergo stretch. It

is found that there is a higher inverse correlation between the elongation of circumferential specimens and the shrinkage along the thickness than along the width, Table 2. After deformation recovery, the specimens show levels of permanent deformation in both thickness and width as neither recovers the initial values for the unstretched specimen, Table 2. Particularly, the thickness shows higher permanent deformation than the width does, which can be attributed to the fact that the fibrillar network is oriented off angle from the circumferential direction and so the deformation of the fibers has a component in the width direction. Whereas in the thickness direction, the shrinkage effects are more from squeezing water out of extracellular matrix during the stretching of the specimen. Comparing the native and extraccelular matrix specimens, Table 2 indicates that the elastin-isolated specimens show higher shrinkage in width and thickness as well as higher recovery, which can be due to higher relative contribution of elastic properties.

In the microstructural domain, first a remark should be made about the loading and unloading protocols adapted here to test the histology of specimens. Although it is sought to chemically fix the microstructure of the tissue specimens at different states during stretch and after deformation recovery, there would still be stress relaxation taking place inside the fixative agent. This is because the fixative agent takes few hours to fully take effect and meanwhile the specimens continue to stress-relax. As a result, what is captured here as the histology of tissue specimens under specific stretch or after deformation recovery might not be accurately described. However, given that the major part of our analysis is on a comparative basis between different loading states, the current protocol provides measures to describe the deformation mechanisms. The test protocols can be improved by developing better fixative agents in order to obtain a more efficient and quick method to fix the tissue microstructure and minimize the post-fixation relaxation.

The first step in our approach to study the microstructural changes was to find the best plane for sectioning the tissue specimens. Given the almost circumferential orientation of fibrillar network around the aorta, the r–z plane is intuitively not a proper sectioning plane since it is technically crossing the fibers and not lying along them. As discussed, the r–θ sections best represent the fibrillar structure in the media layer, but at the same time, the r–θ sections show cross-sectional microstructure in the intima layer, Fig. 7(a). Looking at the similar r–z sections, the pattern is almost reversed as they show cross-sectioning in the media which transits into fibrillar orientation toward the intima, Fig. 7(d). Observations in both planes suggest that the dominant orientation of the fibers is changing from circumferential within the media layer into axial in the intima layer. The dominant circumferential orientation of the fibrillar network in the aortic wall media has long been known and attributed to strengthening the tissue in the circumferential orientation where the maximum stress is experienced due to blood pressure-induced dilation of the aorta. However, longitudinal orientation of the fibrillar structure in the intimal layer has hardly been noticed before. To the best of the author's knowledge, it is the first time that such revealing histology images are obtained to highlight the change in orientation of the fibrillar network when moving from the media to the intima layer. Similar to a physiologically-sound rationale for maximizing the strength of the aortic tissue at the wall media layer when circumferential stress is the largest wall stress, the longitudinal orientation of the fibrillar network in the intima regions can be attributed to increasing tissue strength against maximum stress from shear force caused by blood flow.

The histology results further show how the microstructure changes when tissue-scale deformations take place, Figs. 7(a) through 7(f). Given that it is extremely thin and that it does not have any measurable effects in the biomechanics of the tissue in the circumferential direction, the endothelial layer is not considered in microstructural studying. The r–θ histology of the released specimen, Fig. 7(a), shows a relatively organized set of crimping elastin

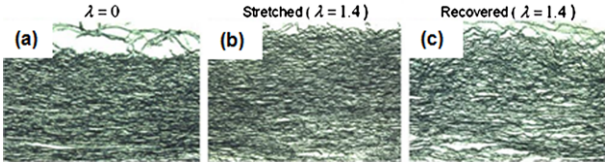

Fig. 10 Histology of specimens from wall "inner" thickness of "elastin-isolated" tissue. (**a**) Unloaded; (**b**) under 1.4 stretch; (**c**) under 2.0 stretch; (**d**) after recovery from 1.4 stretch; (**e**) after recovery from 2.0 stretch

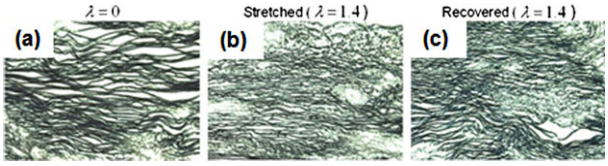

Fig. 11 Histology of specimens from wall "outer" thickness of "elastin-isolated" tissue. (**a**) Unloaded; (**b**) under 1.4 stretch; (**c**) under 2.0 stretch; (**d**) after recovery from 1.4 stretch; (**e**) after recovery from 2.0 stretch

fibrils, and they turn into a more oriented elastin network with drastically less crimping when the specimen is extended, Fig. 7(b). For the specimens recovered from extension, Fig. 7(c), the microstructure takes a highly disorganized pattern with an increasing degree of crimping, higher than that in the initial released specimen. However, although it is already figured out that the histological quantification should rely on r–θ histology sections, observations in r–z sections still provide some qualitative understanding of microstructural deformations. For instance, the specimen in extension shows a uniform pattern of small cross sections, Fig. 7(e), compared to larger clots of (inclined) cross sections in released samples, Fig. 7(d), which indicates that fibrils get thinner under stretch.

In examining the microstructural changes in the tissue, given that the density of elastin is much higher toward the inner media compared to the outer media/adventitia, histological examinations were separately conducted on $1/3$ inner wall thickness and $1/3$ outer wall thickness. The observations on inner media are expected to be more representative of elastin biomechanics. The histological examinations of the tissue specimens under no stretch, stretches of 1.4 and 2.0 and after deformation recovery from stretches 1.4 and 2.0 shed light on morphological mechanisms of deformation at the microstructural scale. The networks in the wall inner layer show straighter fibrillar structure under stretch, which partly returns to the crimping structure after deformation recovery, Fig. 8. The fibrillar network in the wall outer layer shows a more undulated network, Fig. 9, which is hypothetically due to the sparser extracellular matrix, which allows free configuration of the network. Similar patterns are seen for elastin-isolated tissue, Figs. 10 and 11, with higher levels of crimping in the elastin network, which again could be due to the sparser extracellular matrix after digesting the non-elastin components.

The possibility of permanent deformations being generated under physiologic loads is unlikely to occur in vivo. However, it is important to keep in mind that these tissues are excised from the animal and placed in an artificial environment. Unfortunately, this is a necessary step, as there is currently no method to perform such measurements in situ. In this current configuration, the microstructure has already been compromised by cuts made in preparing the specimens. Thus, any constraints on the fibrous proteins that might restore the

tissue are likely lost. There is also blood pressure and blood flow occurring in the complex physiologic environment. Both convection and diffusional transport may play a significant role in osmotic pressure within the tissue. While our configuration does not take these factors into account, it also does not suffer from any potential confounds that might arise from them. This allowed us to control the hydration and mechanical loads more precisely. We believe the take-home message from this study is that these data provide a better idea of the relative contributions of elastin and other matrix proteins, such as collagen, during tissue deformation. The absolute numbers we obtained may need to be adjusted for translating to an in vivo setting.

Acknowledgements We would like to gratefully thank Dr. Hugh Bruck from the Department of Mechanical Engineering at the University of Maryland, College Park, for his intellectual contributions toward this work. We would also extend our gratitude to Hyunchul Kim for his help during the course of experimentation.

References

Amenabar, J.M., et al.: Comparison between semi-automated segmentation and manual point-counting methods for quantitative analysis of histological sections. J. Oral Sci. **48**, 139–143 (2006)

Apter, J.T.: Correlation of visco-elastic properties with microscopic structure of large arteries: IV. Thermal responses of collagen, elastin, smooth muscle, and intact arteries. Circ. Res. **21**, 901–918 (1967)

Avolio, A., Jones, D., Tafazzoli-Shadpour, M.: Quantification of alterations in structure and function of elastin in the arterial media. Hypertension **32**, 170–175 (1998)

Bergel, D.H.: The visco-elastic properties of the arterial wall. PhD dissertation, University of London, London, UK (1960)

Bolender, R.P.: Biological stereology: history, present state, future directions. Microsc. Res. Tech. **21**, 255–261 (1992)

Brunt, E.M.: Grading and staging the histopathol lesions of chronic hepatitis: Knodell histology activity index and beyond. Hepatology **31**, 241–246 (2000)

Brzezinski, J., Oszkinis, G., Marzec, E.: Dielectric relaxation of a protein-water system in atherosclerotic artery wall. Med. Biol. Eng. Comput. **45**, 525–529 (2007)

Castleman, K.R.: Digital Image Processing, pp. 15–72. Prentice-Hall, New York (1996)

Dahab, G.M., et al.: Digital quant of fibrosis in liver biopsy sections: description of a new method by Photoshop software. Gastroenterol. Hepatol. **19**, 78–85 (2004)

Daniels, F., et al.: Quantification of collagen orientation in 3D engineered tissue. In: IFMBE Proceedings, 3rd Kuala Lumpur International Conference on Biomedical Engineering, vol. 15, pp. 282–285 (2006)

Erikson, A., et al.: Quantification of the second-order nonlinear susceptibility of collagen I using a laser scanning microscope. Biomed. Opt. **12**, 044002/1–044002/10 (2007)

Fung, Y.C.: Biomechanics: Mechanical Properties of Living Tissues, 2nd edn. Springer, New York (1993)

Gravey, W., et al.: A modified Verhoeff elastic Van Geieson stain. J. Histotechnol. **14**, 113–114 (1991)

He, C.M., Roach, M.R.: The composition and mechanical properties of abdominal aortic aneurysms. Vasc. Surg. **20**, 6–13 (1994)

Hoeve, C.A.J., Flory, P.J.: The elastic properties of elastin. Appl. Phys. **80**, 6523–6526 (1958)

Hopwood, D.: Some aspects of fixation with glutaral. J. Anat. **101**, 83–92 (1967)

Humphrey, J.D.: An evaluation of pseudoelastic descriptors used in arterial mechanics. J. Biomech. Eng. **121**, 259–262 (1999)

Ishak, K., et al.: Histological grading and staging of chronic hepatitis. J. Hepatol. **22**, 696–699 (1995)

Kage, M., et al.: Long-term evolution of fibrosis from chronic hepatitis to cirrhosis in patients with hepatitis C: morphometric analysis of repeated biopsies. J. Hepatol. **25**, 1028–1031 (1997)

Knodell, R.G., et al.: Formulation and application of a numerical scoring system for assessing histological activity in asymptomatic chronic active hepatitis. J. Hepatol. **1**, 431–435 (1981)

Lillie, M.A.: PhD dissertation, Univ. of Western Ontario, London, Canada (1986)

Lillie, M.A., Chalmers, G.W.G., Gosline, J.M.: The effects of heating on the mechanical properties of arterial elastin. Connect. Tissue Res. **31**, 23–35 (1994)

Lillie, M.A., Chalmers, G.W.G., Gosline, J.M.: Elastin dehydration through the liquid and the vapor phase: a comparison of osmotic stress models. Biopolymers **39**, 627–639 (1996)

Pezzin, G., Scandola, M., Gotte, L.: The low-temperature mechanical relaxation of elastin: I. The dry protein. Biopolymers **15**, 283–292 (1976)
Roberts, N., Puddephat, M.J., McNulty, V.: The benefit of stereology for quantitative radiology. Br. J. Radiol. **73**, 679–697 (2000)
Rubbens, M.P., et al.: Quantification of the temporal evolution of collagen orientation in mechanically conditioned engineered cardiovascular tissues. Ann. Biomed. Eng. **37**, 1263–1272 (2009)
Samouillan, V.A., et al.: Characterization of elastin and collagen in aortic bioprostheses. Med. Biol. Eng. Comput. **38**, 226–231 (2000)
Shahmirzadi, D., Hsieh, A.H., Haslach, H.W.: Effects of arterial tissue storage and burst failure on residual stress relaxation. In: 34th Annual Northeast Bioengineering Conf., Providence, 4–6 April 2008
Shahmirzadi, D., Hsieh, A.H.: Characterizing deformation-induced changes in aortic microstructure using image processing techniques. In: SEM Fall Symposium and Workshop on Advanced Image-Based Measurement Methods, Columbia, SC, 5–7 October 2009a
Shahmirzadi, D., Hsieh, A.H.: microstructural deformations of arterial tissue under stress relaxation and deformation recovery. In: BMES Annual Fall Scientific Meeting, Pittsburgh, PA, 7–10 October 2009b
Shahmirzadi, D., Hsieh, A.H.: Tissue- and microstructural-level deformation of aortic tissue under viscoelastic/viscoplastic loading. In: SEM Annual Conf. and Exposition on Exp. and Applied Mechanics, Indianapolis, IN, 7–9 June 2010
Shahmirzadi, D., Bruck, H., Hsieh, A.H.: Image-based quantification of microstructural alterations in undeformed, stretched and recovered specimens from native and elastin-isolated aqortic tissues, submitted (a)
Shahmirzadi, D., Bruck, H., Hsieh, A.H.: Effects of ECM hydration and composition on vascular tissue viscoelasticity, submitted (b)
Sheehan, D.C., Hrapchak, B.B.: Theory and Practice of Histotechnology, pp. 190–191. The Moxby Company, St. Louis (1980),
Sun, W., et al.: Nonlinear optical microscopy: use of second harmonic generation and two-photon microscopy for automated quantitative liver fibrosis studies. J. Biomed. Opt. **13**, 064010/1–064010/7 (2008)
Tonar, Z., et al.: Microscopic image analysis of elastin network in samples of normal, atherosclerotic and aneurysmatic abdominal aorta and its biomechanical implications. J. Appl. Biomed. **1**, 149–159 (2003)
Vaishnav, R.N., Vossoughi, J.: Residual stress and strain in aortic segments. J. Biomech. **20**, 235–239 (1987)
Vosoughi, J., et al.: Intimal residual stress and strain in large arteries. In: ASME Advances in Bioengineering, pp. 434–437 (1993)
Weibel, E.R.: Measuring through the microscope: development and evolution of stereological methods. J. Microsc. **155**, 393–403 (1989)
Weinberg, P.D., Winlove, C.P., Parker, K.H.: The distribution of water in arterial elastin: effects of mechanical stress, osmotic pressure, and temperature. Biopolymers **35**, 161–169 (1995)
Weinberg, E.J., Shahmirzadi, D., Mofrad, M.R.K.: On the multiscale modeling of heart valve in health and disease. Biomech. Model. Mechanobiol. **9**(4), 373–387 (2010)
Wright, N.T., Humphrey, J.D.: Denaturation of collagen via heating: an irreversible rate process. Annu. Rev. Biomed. Eng. **4**, 109–128 (2002)